CALIBRATION OF THE ROBOTIC ARM WITH CORRECTIONS USING LOCAL LINEAR NEURO-FUZZY MODELS

PETR BENES[1], JAN HLADIK[1], JAN PELIKAN[1], ZDENEK NEUSSER[1], MARTIN NECAS[1], JIRI SVEDA[2], MICHAEL VALASEK[1], ZBYNEK SIKA[1]

[1]Czech technical university in Prague, Faculty of Mechanical Engineering, Department of Mechanics, Biomechanics and Mechatronics, Prague, Czech Republic

[2]Czech technical university in Prague, Faculty of Mechanical Engineering, Department of production machines and equipment (RCMT), Prague, Czech Republic

DOI: 10.17973/MMSJ.2022_12_2022160

e-mail to corresponding author: petr.benes@fs.cvut.cz

The paper deals with the enhancement of the robotic arm calibration using corrections based on local linear neuro-fuzzy models. After the standard calibration of the geometric parameters in the robot's kinematic model, there are still residual errors between the measured positions and the positions predicted by the model. The source of these errors are various non-geometric parameters and nonlinear phenomena that traditional kinematic calibration models do not include. The neuro-fuzzy model based on a locally linear model tree can approximate the residual error as a function of the robot's joint angles. Adding this approximation to the output of the calibrated robot model significantly increases the accuracy of the end-effector position. The results of the described method were verified and compared with other approaches on a simulation model of a flexible planar two-link mechanism. Experimental verification was performed on an industrial robot Stäubli TX200 with data measured by Leica laser tracking device.

KEYWORDS

Robot calibration; Local linear model; Neuro-fuzzy model; Parameter identification; Accuracy of machine positioning

1 INTRODUCTION

Positioning accuracy is one of the basic requirements for manipulators, robots and production machines. To meet this requirement, the actual values of the machine parameters must be entered in the control system. These differ from the nominal design dimensions due to manufacturing and assembly errors. The process of determining the actual machine parameters is called calibration [Mooring 1991], [Mao 2019]. The standard for the serial kinematic mechanisms (SKM) is kinematic calibration based on measuring the position of the machine's end effector with an accurate external measuring device and at the same time recording the positions of the drives measured by their internal sensors. It is then possible to calculate the required parameters from the equations of the kinematic loops. In the case of parallel kinematic mechanisms (PKM) with non-minimum number of sensors it is also possible to perform self-calibration [Sika 2012] without an external measuring device.

However, the kinematic model does not contain non-geometric errors such as the stiffness error, thermal error, gear backlashes etc. More sophisticated calibration approaches have been introduced to address these issues. Elasto-geometrical calibration using identification models is used in [Jiang 2021] and [Mei 2021]. The selection of poses for robot elasto-static calibration is presented in [Kalas 2021]. Another elastic calibration approach uses flexible-rigid coupling error in the non-kinematic calibration with additional optimisation process [Xiaoyan 2019]. A projection technique as a special transformation of kinematic structure is also a possible approach which expresses the nonlinear behaviour and elasticity of the mechanism under the different input loadings [Jeon 2010]. Another way could be the pseudo-error theory which is proposed by considering multiple sources of errors as a single hypothetical error source, which only causes the deflection of joint variables [Zhang 2012]. In [Kong 2022] machine learning is proposed as novel nonlinear error compensation. Standard neural networks are used to reduce non-geometric errors in [Aoyagi 2010], [Jang 2001], [Wang 2019], [Song 2022]. However, these and similar methods differ from the presented procedure described in this paper, which is based on a recursively generated local linear model tree (LLMT). The concept of linear models with growing complexity has been used for description of joint shape imperfection in PKMs in [Skopec 2016].

The proper model of kinematic structure has a high influence for the calibration process as well as the model description [Yang 2014]. Even the proper notation is important, e.g. the quaternion used for the model description can be more suitable choice due to the singularities than other methods [Wang 2018], [Li 2019], [Fu 2020].

The measurement itself has a great influence for the whole calibration process [Wang 2017], [Du 2014], [Santolaria 2013]. For the SKMs the extern calibration devices were introduced [Nubiola 2014], [Yang 2020] to close the open kinematic chain. These extra added mechanisms for the calibration purpose could be a substitution for laser tracker [Aoyagi 2010] or other measuring devices such as specialized redundant calibration machine RedCaM [Benes 2008]. Another substitution of the laser tracker was introduced by the low-cost wire-sensor system places at the end effector platform [Legnani 2014]. Due to the vision improvement in connection with a higher computational performance a camera plays a great role in position determination and machine calibration [Nissler 2017], [Abdullah 2019], [Wu 2019], [Gao 2022]. A closer problem is a calibration of the sensor itself which is needed for a camera sensor type to determine its accurate location on a mechanism [Condurache 2016]. In this paper experimental measurements were performed using the absolute laser tracking device.

2 LOCAL LINEAR NEURO-FUZZY MODELS

The neuro-fuzzy (NF) model is based on the set of local linear models (LLM) with associated fuzzy validity functions that determine the region of validity of each particular model. The output $\hat{y}$ is defined as a weighted sum of LLMs outputs [Nelles 2000]

$$\hat{y} = \sum_{i=1}^{M} \left(w_{i0} + w_{i1}u_1 + \cdots + w_{ip}u_p\right) \Phi_i(\boldsymbol{u}), \tag{1}$$

where $\boldsymbol{u} = \left[u_1, u_2, \cdots, u_p\right]^{\boldsymbol{T}}$ is the vector of inputs, M is the number of LLMs, w_{ij} are linear parameters of i-th LLM. $\Phi_i(\boldsymbol{u})$ is the input-dependent normalized validity function of i-th LLM. The validity function is typically normalized Gaussians and form a partition of unity [Nelles 2000]

$$\sum_{i=1}^{M} \Phi_i(\boldsymbol{u}) = 1. \tag{2}$$

The learning task of the neural network can be written as a regression problem. The goal of regression analysis is to find an approximation function that minimizes the selected cost function, e.g. the sum of squares of errors, on the learning data set. The approximation function can be expressed using a linear model tree. More precisely, a binary decision tree with a linear model in each leaf, where each inner node of the tree structure contains a splitting rule that divides the data into two subsets [Potts 2005]. The batch algorithm for building tree from a training data set starts at the root and performs top-down induction. The data set is split recursively until the tree is sufficiently accurate or other criteria that stop splitting are met. The splitting rule was based on the difference in residual sums of squares (RD). The selected area is first approximated by one linear model. In the case of a sufficient number of samples, the area is divided into two sub-areas with their own linear models. If the increase in accuracy achieved by splitting is significant, the split is stored in a tree structure. The process continues until the desired accuracy is achieved throughout the workspace.

For our task, we used a non-incremental form of the batch-RD algorithm called the Incremental model tree induction (IMTI) with RD splitting rule based on the RETIS algorithm [Karlic 1992]. This algorithm covers the input space by discontinuous (non-consecutive) linear models. A continuous variant with smoothing using validity functions was also tested. However, this smoothing results in a noticeable deterioration in the accuracy of the model, and it has not been used (similarly to [Potts 2005]).

3 BASIC ALGORITHM OF CALIBRATION

The kinematic structure is described in given position using kinematic constraints in the form

$$\boldsymbol{f}(\boldsymbol{d},\boldsymbol{s},\boldsymbol{w}) = \boldsymbol{0}, \tag{3}$$

where $\boldsymbol{d}$ are the parameters to be calibrated, $\boldsymbol{s}$ are the measured coordinates in the joints and $\boldsymbol{w}$ are the output coordinates, e.g., end-effector coordinates. Parameters include the geometry (dimensions) of the links and some parameters of the sensors (such as offsets). Considering n measured positions the constraints (3) are coupled into the form

$$\boldsymbol{F}(\boldsymbol{d},\boldsymbol{S},\boldsymbol{W}) = \boldsymbol{0}, \tag{4}$$

$$\boldsymbol{F} = [\boldsymbol{f}_1,\dots,\boldsymbol{f}_n]^T; \boldsymbol{S} = [\boldsymbol{s}_1,\dots,\boldsymbol{s}_n]^T; \boldsymbol{W} = [\boldsymbol{w}_1,\dots,\boldsymbol{w}_n]^T. \tag{5}$$

The calibration parameters $\boldsymbol{d}$ are the same for all positions, but their real manufactured values $\bar{\boldsymbol{d}}$ differ from design values. If n is higher than the number of calibrated parameters, the equation (4) represents over-constrained system of nonlinear algebraic equations. The calibration algorithm [Sika 2012] is based on the modified Newton's method derived using the Taylor series of (4)

$$\boldsymbol{F}(\bar{\boldsymbol{d}},\boldsymbol{S},\boldsymbol{W}) + \boldsymbol{J}_{\boldsymbol{d}}\partial\boldsymbol{d} + \dots = \boldsymbol{0}, \tag{6}$$

where $\boldsymbol{J}_{\boldsymbol{d}}$ is the Jacobi matrix of partial derivatives of (4) with respect to $\boldsymbol{d}$. Using the first term of the Taylor series, equation (6) can be rewritten in the form

$$\boldsymbol{J}_{\boldsymbol{d}}\partial\boldsymbol{d} = -\boldsymbol{F}(\bar{\boldsymbol{d}},\boldsymbol{S},\boldsymbol{W}) = \partial\boldsymbol{r} \tag{7}$$

and the *i*-th iteration step of Newton's method is

$$\partial\boldsymbol{d}_i = (\boldsymbol{J}_{\boldsymbol{di}}{}^{\boldsymbol{T}}\boldsymbol{J}_{\boldsymbol{di}})^{-1}\boldsymbol{J}_{\boldsymbol{di}}{}^{\boldsymbol{T}}\partial\boldsymbol{r}_i, \tag{8}$$

where $\boldsymbol{J}_{\boldsymbol{di}}$ is the Jacobi matrix, $\partial\boldsymbol{r}_{\boldsymbol{i}} = -\boldsymbol{F}(\boldsymbol{d}_{\boldsymbol{i}},\boldsymbol{S},\boldsymbol{W})$ is the vector of deviations computed from measured quantities and calibrated quantities from the previous iteration step. The new values of calibrated parameters are computed

$$\boldsymbol{d}_{i+1} = \boldsymbol{d}_i + \partial\boldsymbol{d}_i. \tag{9}$$

The iterations continue as long as the deviations are decreasing. Usually about 5 or 6 iteration steps are sufficient.

4 REFERENCE MODEL

To compare the accuracy of the considered approaches, it was first necessary to create a reference model that represents the real behaviour of the manipulator. A flexible planar two-link mechanism was chosen, Fig. 1. The links are considered as flexible beams in the gravity field. The mass of both links and the added mass M at point C are considered. An analytical model was created whose outputs are used as equivalent to measurements performed on a real manipulator using an external measuring device, e.g., laser tracker.

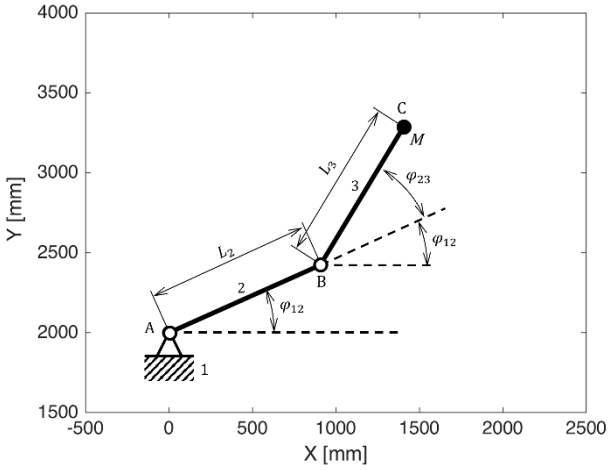

Figure 1. Planar two-link manipulator

Both links are considered as round bars with diameter $d = 60\ mm$, made of steel $\rho = 7850\ kg/m^3$, $E = 210\ GPa$, gravitational acceleration $g = 9{,}81\ m/s$ and end point mass $M = 10\ kg$. Both links have the same length $L_2 = L_3 = 1000\ mm$.

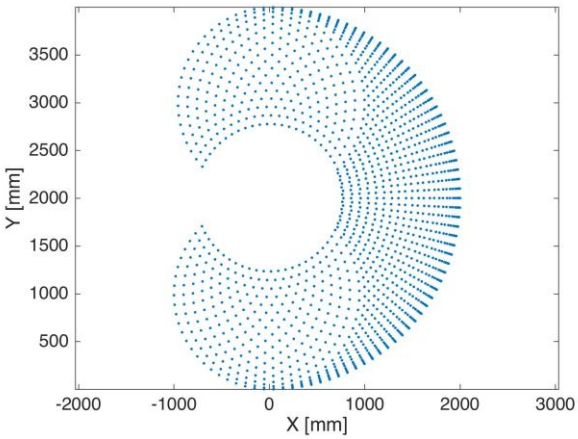

Figure 2. Manipulator workspace

The origin of the manipulator, point A, was placed on the coordinates $X_A = 0\ mm, Y_A = 2000\ mm$. The workspace for the considered range of angles $\varphi_{12} \in \langle -\pi/2; \pi/2 \rangle$, $\varphi_{23} \in \langle -3\pi/4; 3\pi/4 \rangle$ is shown in Fig. 2. A total of 1536 positions of the end point $C = [\tilde{X}_C, \tilde{Y}_C]$ were calculated, evenly distributed in the workspace. This data set was used for calibrations as well as a training set for the synthesis of neuro-fuzzy models.

5 RIGID KINEMATIC MODEL

The first model created is a rigid kinematic model. The bodies are considered rigid and straight. The input of the model is the angle φ_{12} between the base frame and body number 2 and the angle φ_{23} of rotation of body 3 relative to body 2. The model parameters are the coordinates of point $A\ [X_A, Y_A]$ and the length of links L_2, L_3. The outputs are the coordinates of point $C\ [X_C, Y_C]$. The relation applies to the position of point C:

$$X_C = X_A + L_2\ cos(\varphi_{12}) + L_3\ cos(\varphi_{12} + \varphi_{23}), \tag{10}$$

$$Y_C = Y_A + L_2\ sin(\varphi_{12}) + L_3\ sin(\varphi_{12} + \varphi_{23}). \tag{11}$$

6 CALIBRATED RIGID KINEMATIC MODEL

The second model has been extended by calibration parameters. We assume that both links are rigid, but not perfectly straight. Their description has been modified for calibration purposes according to the structure in Fig. 3.

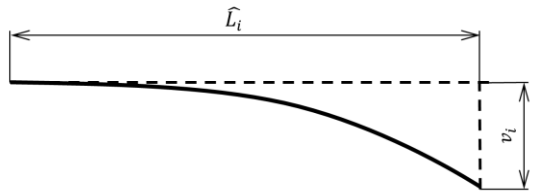

Figure 3. Link model with calibration parameters

The position of the end effector point C is described by equations (12), (13) that represent a calibrated model with the set of calibration parameters $\boldsymbol{d} = [\widehat{L_2}, \widehat{L_3}, v_2, v_3]$ and the measured values on the internal sensors of the mechanism $\boldsymbol{s} = [\varphi_{12}, \varphi_{23}]$. This set of calibration parameters is also able to describe the possible offset of the sensors.

$$\begin{aligned} X_C = X_A + \widehat{L_2}\ cos(\varphi_{12}) + v_2\ cos\left(\varphi_{12} + \tfrac{3\pi}{2}\right) + \\ + \widehat{L_3}\ cos(\varphi_{12} + \varphi_{23}) + v_3\ cos\left(\varphi_{12} + \varphi_{23} + \tfrac{3\pi}{2}\right), \end{aligned} \tag{12}$$

$$\begin{aligned} Y_C = Y_A + \widehat{L_2}\ sin(\varphi_{12}) + v_2\ sin\left(\varphi_{12} + \tfrac{3\pi}{2}\right) + \\ + \widehat{L_3}\ sin(\varphi_{12} + \varphi_{23}) + v_3\ sin\left(\varphi_{12} + \varphi_{23} + \tfrac{3\pi}{2}\right). \end{aligned} \tag{13}$$

The kinematic constraints for calibration referring to equation (3) have the form

$$\begin{aligned} f_1 = X_A + \widehat{L_2}\ cos(\varphi_{12}) + v_2\ cos\left(\varphi_{12} + \tfrac{3\pi}{2}\right) + \\ + \widehat{L_3}\ cos(\varphi_{12} + \varphi_{23}) + v_3\ cos\left(\varphi_{12} + \varphi_{23} + \tfrac{3\pi}{2}\right) - \\ - \tilde{X}_C = 0, \end{aligned} \tag{14}$$

$$\begin{aligned} f_2 = Y_A + \widehat{L_2}\ sin(\varphi_{12}) + v_2\ sin\left(\varphi_{12} + \tfrac{3\pi}{2}\right) + \\ + \widehat{L_3}\ sin(\varphi_{12} + \varphi_{23}) + v_3\ sin\left(\varphi_{12} + \varphi_{23} + \tfrac{3\pi}{2}\right) - \\ - \tilde{Y}_C = 0. \end{aligned} \tag{15}$$

The parameters $\tilde{X}_C$ and $\tilde{Y}_C$ correspond from the calibration point of view to the values measured by the external measuring instrument. The calibrability number [Sika 2012] for this task was 1.78, which indicates a very good conditionality and numerical stability of the calculation. This was also proved by the fact that the iteration algorithm converged to the solution already in the second iteration. The calibrated parameters came out as follows: $\widehat{L_2} = 1000\ mm$, $\widehat{L_3} = 999.998\ mm$, $v_2 = 0.41\ mm$, $v_3 = 0.36\ mm$.

7 CALIBRATED RIGID KINEMATIC MODEL WITH CORRECTIONS USING NEURO-FUZZY MODELS

The basis of the next model is the calibrated model from the previous section, which is supplemented by the position error correction against the exact measured values. In simulation these are represented by the data from the flexible model.

First, the error functions in the x and y axis direction are expressed:

$$e_x(\varphi_{12}, \varphi_{23}) = \tilde{X}_C - X_C, \tag{16}$$

$$e_y(\varphi_{12}, \varphi_{23}) = \tilde{Y}_C - Y_C. \tag{17}$$

The error values for the prescribed inputs φ_{12} and φ_{23} are shown in Fig. 4 and Fig. 5. These values were used to create approximation models using the local linear model trees method.

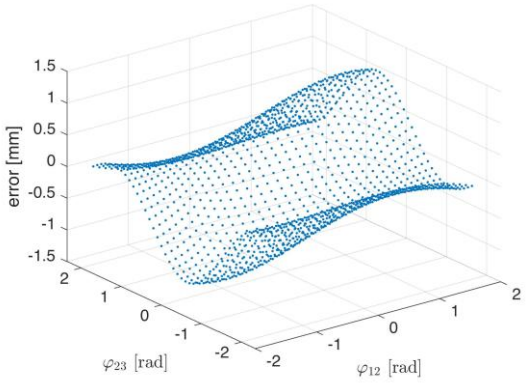

Figure 4. Position error e_x

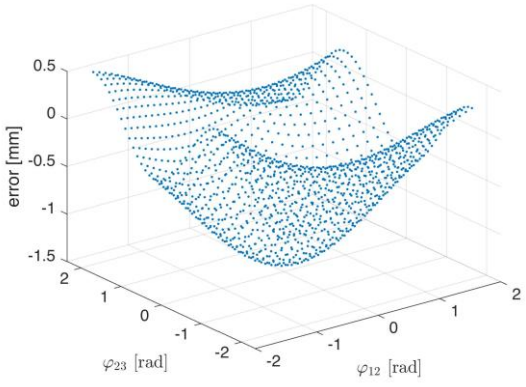

Figure 5. Position error e_y

If we denote the output of the error approximation of individual axes, calculated from linear model trees, as $\tilde{e}_x\ (\varphi_{12}, \varphi_{23})$ and $\tilde{e}_y\ (\varphi_{12}, \varphi_{23})$ the corrected output positions of point C can be defined as:

$$X_{Ccor}(\varphi_{12}, \varphi_{23}) = X_C(\varphi_{12}, \varphi_{23}) + \tilde{e}_x(\varphi_{12}, \varphi_{23})\ , \tag{18}$$

$$Y_{Ccor}(\varphi_{12}, \varphi_{23}) = Y_C(\varphi_{12}, \varphi_{23}) + \tilde{e}_y(\varphi_{12}, \varphi_{23}). \tag{19}$$

This correction uses 93 linear models to determine $\tilde{e}_x$ and 75 models for $\tilde{e}_y$, see Fig. 6 and Fig. 7. Further increasing the number of models improved the approximation accuracy by less than 2 %, which was the chosen threshold.

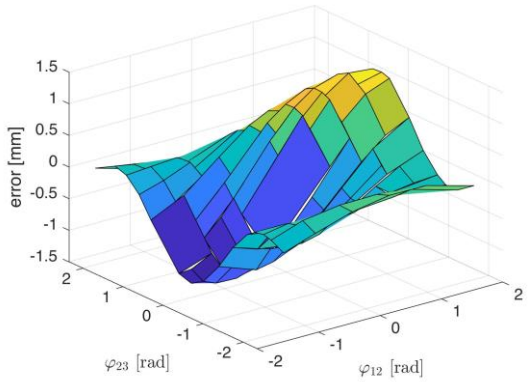

Figure 6. LLMT models for error approximation $\tilde{e}_x$

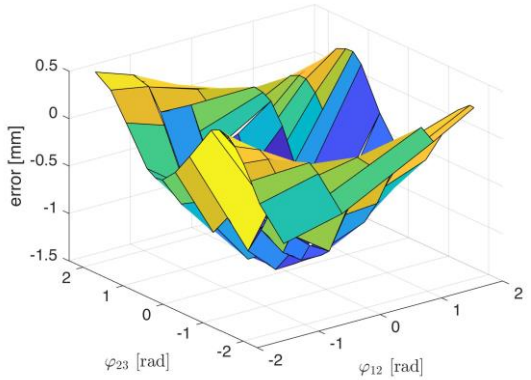

Figure 7. LLMT models for error approximation $\tilde{e}_y$

8 FLEXIBLE MODEL REALIZED ONLY BY FUZZY MODELS

The last model of the planar mechanism uses a "black box" approach. No knowledge of model structure is used. The aim is to approximate the whole flexible model from section 5 only by using the knowledge of its inputs and outputs.

A learning dataset with 1536 positions of the end point C, evenly distributed in the workspace for the given range of angles φ_{12} and φ_{23}, was used. These positions were calculated using the flexible model from section 4. Approximations were generated from this learning dataset using linear model trees. There were 211 linear models recursively generated for the x axis and 209 for the y axis. In this case, the number of models was mainly determined by the number of learning positions. In the areas with the largest error, there were not enough points to reduce it further. The models are shown in Fig. 8 and Fig. 9.

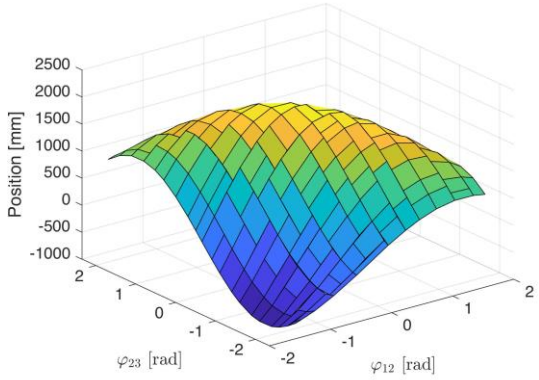

Figure 8. Fuzzy model - position X_C

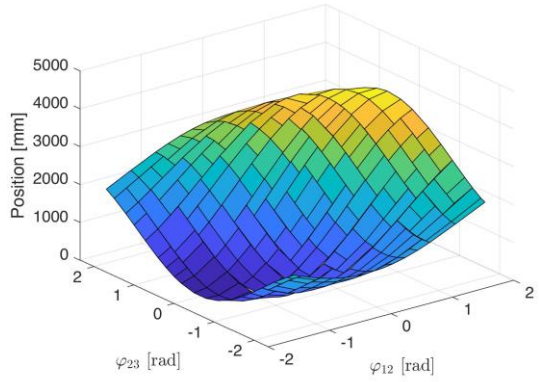

Figure 9. Fuzzy model - position Y_C

9 COMPARISON OF MODELS

A new testing dataset was created to compare all models. If a comparison were made on the learning dataset, only information on the success of the approximation at the given points would be obtained. The testing data set contained 5985 samples - mechanism positions. An evaluation criterion - total error e_t - was introduced as

$$e_t = \sqrt{\left(\tilde{X}_C - X_C\right)^2 + \left(\tilde{Y}_C - Y_C\right)^2}. \tag{20}$$

The values of total error in individual points of workspace for all described models are shown in Fig. 10.

The rigid kinematic model had the average error over the entire workspace $e_{t\_avg} = 0.643\ mm$ and the maximum value $e_{t\_max} = 1.427\ mm$. The added calibration parameters reduced these values to workspace $e_{t\_avg} = 0.447\ mm$ and $e_{t\_max} = 0.716\ mm$ in the case of the calibrated rigid kinematic model. As expected, the calibrated kinematic model with NF correction achieved the best results from all models, $e_{t\_avg} = 0.0157\ mm$, $e_{t\_max} = 0.131\ mm$.

The result achieved by the pure neuro-fuzzy model is worse by an order of magnitude. The average total error has a value $e_{t\_avg} = 7.877\ mm$ and the maximum error $e_{t\_max} = 42.815\ mm$. However, the accuracy of the model created in this way is greatly affected by the size of the learning set and its distribution in the workspace. This result was obtained from a learning set containing 1536 samples, which was used for all other models. For comparison, a new data set with 148 680 learning samples was created in the same

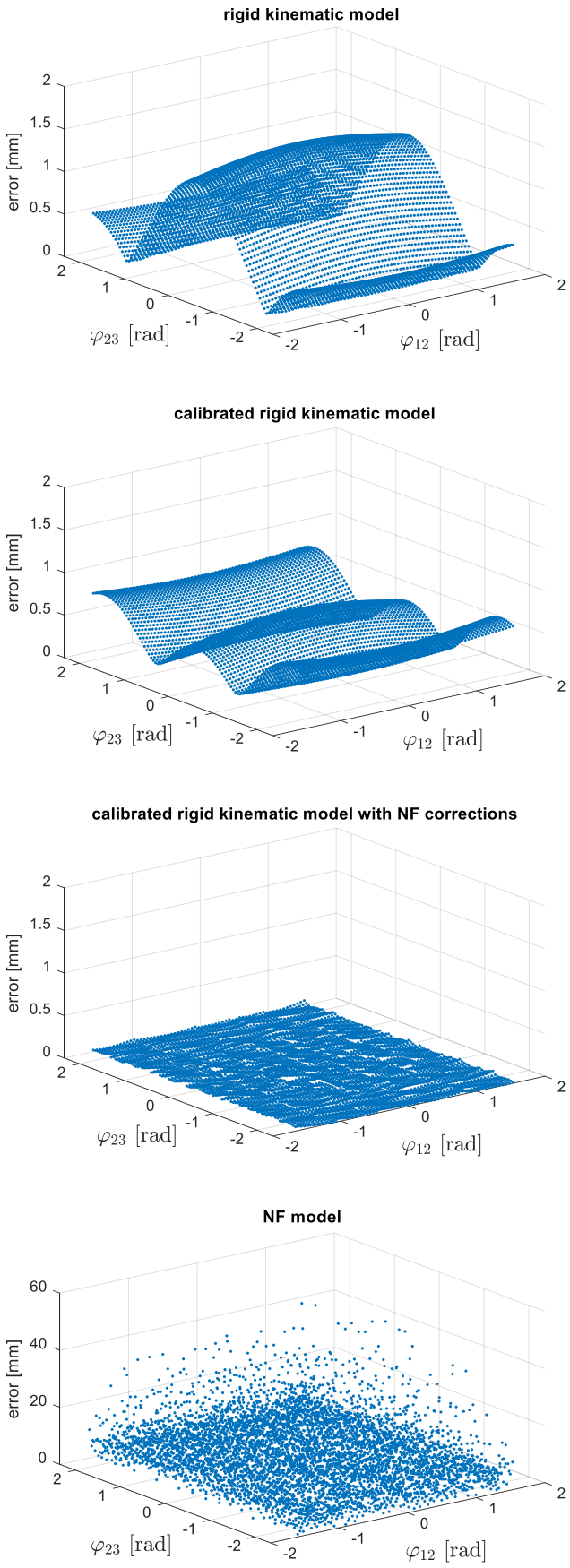

Figure 10. Total error e_t – comparisson of models

workspace. The model created from these data was composed of 3283 linear models for x axis approximation and 3331 models for y axis approximation. The average total output error of this new model was $e_{t\_avg} = 0.406\ mm$ and the maximum error was $e_{t\_max} = 3.299\ mm$. The results are better, but the computational complexity is significantly higher for such a large model. A summary of all results is given in Table 1.

Model	e_{t_avg} [mm]	e_{t_max} [mm]
Rigid kinematic model	0.643	1.427
Calibrated rigid kinematic model	0.447	0.716
Calibrated rigid kinematic model with NF correction	0.016	0.131
NF model (1536 learning points)	7.877	42.815
NF model (148 680 learning points)	0.406	3.299

Table 1. Average and maximum total error values

10 CALIBRATION OF AN INDUSTRIAL ROBOT

The industrial robot Stäubli TX200 was used for experimental verification of the calibration with neuro-fuzzy corrections. It is a fully enclosed six-axis angular robot with a maximum payload of 130 kg and a maximum reach of 2194 mm. The declared repeatability of the robot is 0.06 mm.

The kinematic model of the robot was created using Denavit-Hartenberg (DH) notation. Table 2 shows the parameters taken from the robot control system after the standard calibration procedure.

Axis	α [deg]	a [mm]	d [mm]	θ [deg]
1	0	0	642	0
2	-89.9955	249.2886	450.9658	-90.0587
3	0.0192	950.007	-450	89.9319
4	90.0423	0.6907	800.94	0.0045
5	-90.0598	-0.3995	0	-0.0045

Table 2. Stäubli TX200 DH parameters

The coordinates of the robot's end-effector were measured in 45 different positions using the Leica absolute tracker. The experimental setup is shown in Fig. 11. The recorded data in each position included the coordinates of the end-effector measured by the absolute tracker, the angles of rotation of the drive axes from the integrated sensors and the nominal position of the end-effector calculated by the robot control system. The measured points are shown in Fig. 12. The blue arrows represent the differences between the real position measured by the absolute tracker and the position calculated by the robot control system. The length of the arrow represents the size of the position error, values are 1000x scaled for better clarity.

Figure 11. Experiment – robot Stäubli TX200 and Leica absolute tracker

The distribution of errors in Fig. 12 shows no clear dependencies. This is because the error does not depend directly on the position of the end-effector. Instead, it depends on the positions of the drives. Therefore, we can try to find error functions in the x, y and z axis direction similarly to (16), (17). The inputs are the positions of the robot drives.

Three NF models $\tilde{e}_x$, $\tilde{e}_y$, $\tilde{e}_z$ were created and used for the correction of the position error. Each NF model consisted of five linear models. A comparison of the total position errors of the calibrated robot without NF correction and with NF correction is shown in Fig. 13.

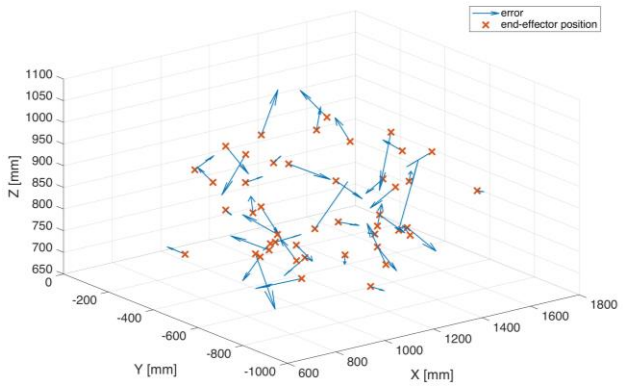

Figure 12. Experiment – measured points and scaled position errors

The average total error of the robot without correction is 0.057 mm, the average total error with NF correction is 0.0126 mm. It is clear from Figure 13 that the NF correction improved the position accuracy in all measured points.

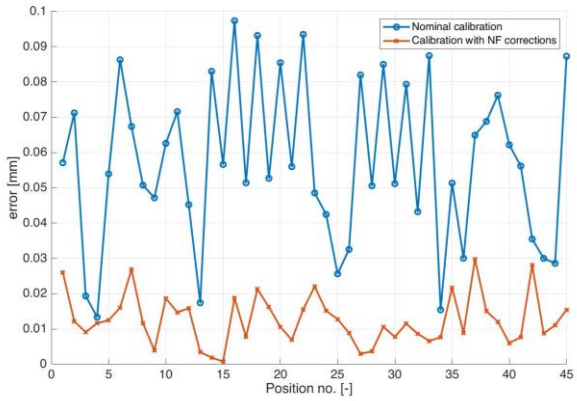

Figure 13. Experiment – position error comparison

11 CONCLUSIONS

This paper describes research into the use of local linear neuro-fuzzy models for the purpose of robotic arm calibration. The basic idea is to use NF correction to eliminate the positioning error of the calibrated robotic arm. The source of this error are various non-geometric phenomena that cannot be covered by traditional kinematic calibration models, such as the flexibility of bodies. The proposed method was compared with traditional calibration approaches. A flexible planar two-link mechanism was considered as a reference model. An order of magnitude better positional accuracy was achieved using NF corrections compared to the traditional calibrated rigid kinematic model. The possibility of using the black-box NF model to solve the entire kinematics of the robot, i.e without any physical basis of the model, was also verified. It has been shown that a large training set and a very large LLMT are needed to achieve comparable results with physically based models. The real verification of the procedure was performed on an industrial robot Stäubli TX200 with the position measured by an external measuring device laser tracker. Using these measured values, a model approximating the endpoint error was created using the LLMT model. This correction reduced the average positioning error five times. The accuracy increased at all measured points. The described position error corrections using LLMT and NF models thus seems to be a very suitable tool for improving traditional kinematic calibration.

ACKNOWLEDGMENTS

This paper has been supported by the project “Manufacturing engineering and precision engineering” funded as project No. CZ.02.1.01/0.0/0.0/16_026/0008404 by OP RDE (ERDF).

REFERENCES

[Abdullah 2019] Abdullah, A. H. et al. A geometric approach for kinematic identification of an industrial robot using a monocular camera. Robotics and Computer Integrated Manufacturing, 2019, 57, pp. 329-346. doi:https://doi.org/10.1016/j.rcim.2018.11.008.

[Aoyagi 2010] Aoyagi, S. et al. Improvement of Robot Accuracy by Calibrating Kinematic Model Using a Laser Tracking System -Compensation of Non-Geometric Errors Using Neural Networks and Selection of Optimal Measuring Points Using Genetic Algorithm. IEEE/RSJ International Conference on Intelligent Robots and Systems, 2010, pp. 5660-5665.

[Benes 2008] Benes, P. et al. Experiments with RedCaM. 25th Danubia-Adria Symposium on Advances in Experimental Mechanics, 2008, pp. 9-10.

[Condurache 2016] Condurache, D., Burlacu, A. Orthogonal dual tensor method for solving the AX = XB sensor calibration problem. Mechanism and Machine Theory, 2016, 104, pp. 382-404.

[Du 2014] Du, G., Zhang, P. Online Serial Manipulator Calibration Based on Multisensory Process Via Extended Kalman and Particle Filters. IEEE TRANSACTIONS ON INDUSTRIAL ELECTRONICS, 2014, 61(12).

[Fu 2020] Fu, Z., T. et al. A dual quaternion-based approach for coordinate calibration of dual robots in collaborative motion. IEEE Robot. Autom. Lett., 2020, 5(3), pp. 4086–4093.

[Gao 2022] Gao, T. et al. Operational kinematic parameter identification of industrial robots based on a motion capture system through the recurrence way. Mechanism and Machine Theory, 2022, 172, doi: 10.1016/j.mechmachtheory.2022.104795.

[Jang 2001] Jang, J. H. et al. Calibration of Geometric and Non-Geometric Errors of an Industrial Robot. Robotica, 2001, 19, pp. 311-321.

[Jeon 2010] Jeon, D. et al. A calibration method of redundantly actuated parallel mechanism machines based on projection technique. CIRP Annals - Manufacturing Technology, 2010, 59, pp. 413-416.

[Jiang 2021] Jiang, Z. et al. Elasto-geometrical calibration of six-DOF serial robots using multiple identification models. Mechanism and Machine Theory, 2021, 157, doi:10.1016/j.mechmachtheory.2020.104211.

[Kalas 2021] Kalas, V. et al. Application-oriented selection of poses and forces for robot elastostatic calibration. Mechanism and Machine Theory, 2021, 159, doi:10.1016/j.mechmachtheory.2020.104176

[Karlic 1992] Karlic, A. Linear Regression in Regression Tree Leaves. In Proceedings of ECAI-92, 1992, pp. 440--441.

[Kong 2022] Kong, L.-B. and Yu, Y. Precision Measurement and Compensation of Kinematic Errors for Industrial Robots Using Artifact and Machine Learning. Adv. Manuf. 2022, 10, 397–410, doi:10.1007/s40436-022-00400-6.

[Lagnani 2014] Legnani, G.,Tiboni, M. Optimal design and application of a low-cost wire-sensor system for the kinematic calibration of industrial manipulators. Mechanism and Machine Theory, 2014, 73, pp. 25-48.

[Li 2019] Li, G. et al. Kinematic calibration of serial robot using dual quaternions. Industrial Robot, 2019, 46(2), pp. 247-258, doi: 10.1108/IR-10-2018-0221.

[Mao 2019] Li, G. et al. A novel algorithm for robust calibration of kinematic manipulators and its experimental validation. IEEE *Access*, 2019, 7, pp. 90487–90496.

[Mei 2021] Mei, B. et al. Elasto-geometrical error modeling and compensation of a five-axis parallel machining robot. Precision Engineering, 2021, 69, pp. 48-61.

[Mooring 1991] Mooring, B. et al. Fundamentals of Manipulator Calibration. New York: Wiley & Sons, 1991.

[Nelles 2000] Nelles, O. et al. Local Linear Model Trees (LOLIMOT) Toolbox. IFAC System Identification. 2000. Santa Barbara, California.

[Nissler 2017] Nissler, C., Marton, Z.C. Robot-to-camera calibration: a generic approach using 6D detections. The 1st IEEE international conference on robotic computing (IRC). 2017. Taichung, pp. 299-302, doi: 10.1109/IRC.2017.66.

[Nubiola 2014] Nubiola, A., Bonev, I. Absolute robot calibration with a single telescoping ballbar. Precision Engineering, 2014, 38, 472-480.

[Potts 2005] Potts, D., Sammut, C. Incremental Learning of Linear Model Trees. Machine Learning, 2005, 61(1), pp. 5-48.

[Santolaria 2013] Santolaria, J., Gine´s, M. Uncertainty estimation in robot kinematic calibration. Robotics and Computer-Integrated Manufacturing, 2013, 29, pp. 370-384.

[Skopec 2016] Skopec, T. et al. Calibration using adaptive model complexity for parallel and fiber-driven mechanisms. Robotica, 2016, 34(6), pp. 1416-14.

[Song 2022] Song, Y. et al. Calibration of a Stewart platform by designing a robust joint compensator with artificial neural networks. Precision Engineering, 2022, 77, pp. 375-384.

[Sika 2012] Sika, Z. et al. Calibrability as additional design criterion of parallel kinematic machines. Mechanism and Machine Theory, 2012, 50, pp. 48–63.

[Wang 2017] Wang, H. et al. Finding Measurement Configurations for Accurate Robot Calibration: Validation With a Cable-Driven Robot. IEEE TRANSACTIONS ON ROBOTICS, 2017, 33(5).

[Wang 2018] Wang, G. et al. A Method of Robot Base Frame Calibration by Using Dual Quaternion Algebra. IEEE *Access*, 2018, 6, pp. 74865-74873, doi: 10.1109/ACCESS.2018.2882502.

[Wang 2019] Wang, Z. et al. A Robot Calibration Method Based on Joint Angle Division and an Artificial Neural Network. Mathematical Problems in Engineering, 2019, Article ID 9293484, doi: 10.1155/2019/9293484.

[Wu 2019] Wu, G., Shi, G. Experimental statics calibration of a multi-constraint parallel continuum robot. Mechanism and Machine Theory, 2019, 136, pp. 72-85.

[Xiaoyan 2019] Xiaoyan, C. Et al. Non-kinematic calibration of industrial robots using a rigid–flexible coupling error model and a full pose measurement method. Robotics and Computer Integrated Manufacturing, 2019, 57, pp. 46-58.

[Yang 2020] Yang, P. et al. Plane kinematic calibration method for industrial robot based on dynamic measurement of double ball bar. Precision Engineering, 2020, 62, pp. 265-272.

[Yang 2014] Yang, X. et al. A minimal kinematic model for serial robot calibration using POE formula. Robotics and Computer-Integrated Manufacturing, 2014, 30, pp. 326-334.

[Zhang 2012] Zhang, D., Gao, Z. Optimal Kinematic Calibration of Parallel Manipulators With Pseudoerror Theory and Cooperative Coevolutionary Network. IEEE TRANSACTIONS ON INDUSTRIAL ELECTRONICS, 59(8).

CONTACTS:

Czech technical university in Prague, Faculty of Mechanical Engineering, Department of Mechanics, Biomechanics and Mechatronics, Technicka 4, 166 07 Praha 4, Czech Republic; Website : https://mech.fsid.cvut.cz/

Ing. Petr Benes, Ph.D.
E: petr.benes@fs.cvut.cz
Ing. Jan Hladik
E: jan.hladik@fs.cvut.cz
Ing. Jan Pelikan, Ph.D.
E: jan.pelikan@fs.cvut.cz
Ing. Zdenek Neusser, Ph.D.
E: zdenek.neusser@fs.cvut.cz
Ing. Martin Necas, Ph.D.
E: martin.necas@fs.cvut.cz
Prof. Ing. Michael Valasek, DrSc.
E: michael.valasek@fs.cvut.cz
Prof. Ing. Zbynek Sika, Ph.D.
E: zbynek.sika@fs.cvut.cz

Czech technical university in Prague, Faculty of Mechanical Engineering, Department of production machines and equipment (RCMT), Horská 3, 128 00 Praha, Czech Republic; Website : https://rcmt.cvut.cz/

Ing. Jiri Sveda, Ph.D.
E: j.sveda@rcmt.cvut.cz